This is the published version of:

Demonstration of synchronised scanning Lidar measurements of 2D velocity fields in a boundary-layer wind tunnel

Demonstration of synchronised scanning Lidar measurements of 2D velocity fields in a boundary-layer wind tunnel

**M F van Dooren[1], M Kühn[1], V Petrović[1,2], C L Bottasso[2,4],
F Campagnolo[2], M Sjöholm[3], N Angelou[3], T Mikkelsen[3],
A Croce[4] and A Zasso[5]**

[1]ForWind, University of Oldenburg, Institute of Physics, Oldenburg, Germany
[2]Wind Energy Institute, Technical University of Munich, Garching, Germany
[3]Dept. of Wind Energy, Technical University of Denmark, Roskilde, Denmark
[4]Dept. of Aerospace Science and Technology, Politecnico di Milano, Milan, Italy
[5]Dept. of Mechanical Engineering, Politecnico di Milano, Milan, Italy

E-mail: `marijn.vandooren@uni-oldenburg.de`

Abstract. This paper combines the currently relevant research methodologies of scaled wind turbine model experiments in wind tunnels with remote-sensing short-range WindScanner Lidar measurement technology. The wind tunnel of the Politecnico di Milano was equipped with three wind turbine models and two short-range WindScanner Lidars to demonstrate the benefits of synchronised scanning Lidars in such experimental surroundings for the first time. The dual-Lidar system can provide fully synchronised trajectory scans with sampling time scales ranging from seconds to minutes. First, staring mode measurements were compared to hot wire probe measurements commonly used in wind tunnels. This yielded goodness of fit coefficients of 0.969 and 0.902 for the 1 Hz averaged u- and v-components of the wind speed, respectively, validating the 2D measurement capability of the Lidar scanners. Subsequently, the measurement of wake profiles on a line as well as wake area scans were executed to illustrate the applicability of Lidar scanning to measuring small scale wind flow effects. The downsides of Lidar with respect to the hot wire probes are the larger measurement probe volume and the loss of some measurements due to moving blades. In contrast, the benefits are the high flexibility in conducting both point measurements and area scanning, and the fact that remote sensing techniques do not disturb the flow while measuring. The research campaign revealed a high potential for using short-range WindScanner Lidar for accurately measuring small scale flow structures in a wind tunnel.

1. Introduction

During the past few years, several research groups have focused attention on wind tunnel experiments with the innovative idea of supporting research not only related to the validation of purely aerodynamic models, but mainly to support numerical activities on control and aero-servo-elasticity [1] as well as understanding the interaction of wind turbines with turbulent flow [2]. In fact, testing of wind turbines in full-scale in the atmospheric boundary-layer imposes several constraints, such as the difficulty in having an accurate knowledge and repeatability of the environmental conditions, higher costs, and especially for public researchers, the difficulty to have access to industrial wind turbines as a research platform. In the same period, academic

and industrial researchers have developed new scanning wind Lidars able to map full three-dimensional vector wind and turbulence fields in 3D space [3],[4],[5]. Even for complex flows, such as the flow around wind turbines, the Lidars can be applied without disturbing the flow itself. The present work reports on the testing activity conducted recently by a team of four research groups, where two short-range WindScanners have been tested in a boundary-layer test section of a wind tunnel for the first time, in order to map the flow of the free chamber as well as to accurately measure the wakes of scaled wind turbine models. This measurement campaign was executed in the scope of the CompactWind project, which has the purpose of investigating the effect of different wind farm control concepts and yaw configurations of the individual turbines on the wind farm energy output, the wake structures and wind turbine loads.

2. Methodology

2.1. The wind tunnel facility

In January 2016, three generically scaled wind turbine models (see figure 1), specifically designed by the Wind Energy Institute (WEI) at the Technical University of Munich (TUM) for wind farm control research applications, as well as two short-range WindScanners (see figure 2) developed by the Department of Wind Energy of the Technical University of Denmark (DTU) were installed in the wind tunnel of the Politecnico di Milano (PoliMi).
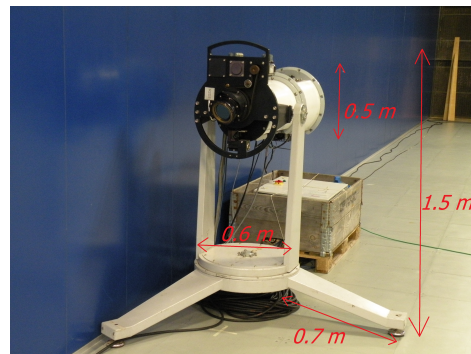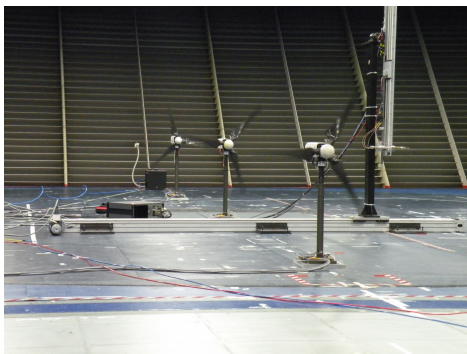
Figure 1. Model wind turbines in operation in the wind tunnel.

Figure 2. One of the two WindScanner Lidars installed in the wind tunnel.
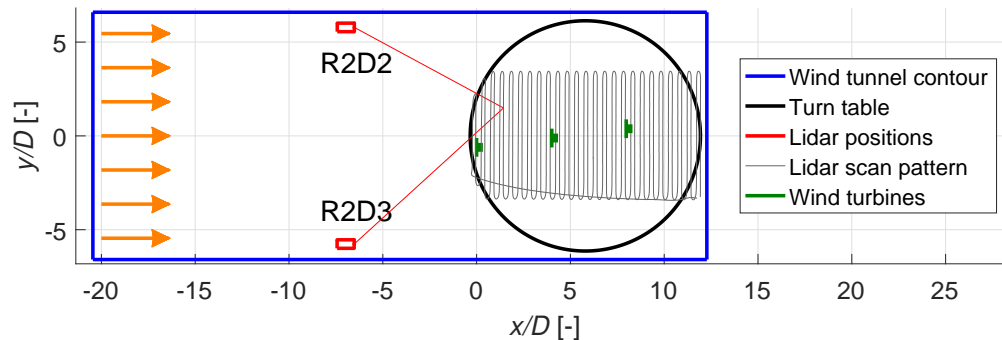

Figure 3. Configuration of the wind tunnel of the Politecnico di Milano with the two scanning Lidars and the three model wind turbines installed on the turn table. The axes are normalised with respect to the wind turbine diameter of $D = 1.1$ m.

The PoliMi wind tunnel has a closed-return configuration facility arranged in a vertical layout with two test sections. The boundary-layer test section, sketched in figure 3, is located at the upper level in the return duct and has a cross-sectional area of 13.84 m by 3.84 m and a length of 36 m, illustrated by the blue outer boundaries in figure 3. The three wind turbines were mounted on a turn table which allows for rotating the entire turbine array setup, as to create a lateral offset between the wind turbines. When the turn table is in its 'home position', the turbines line up in x-direction with a distance of $4D$ between them. The WindScanners are indicated with red rectangles and their commanded synchronised scan pattern for scanning the wind turbine wakes is plotted in grey. Atmospheric boundary-layer conditions can be simulated by the use of turbulence generators, i.e. spires, placed at the chamber inlet at the left boundary. For more information about the wind tunnel, please refer to [6].

2.2. The G1 wind turbine models

The three scaled *G1* wind turbine models have a rotor diameter D of 1.1 m, a hub height of 0.825 m and a rated rotor speed equal to 850 rpm. They were designed to provide a realistic energy conversion process, which means reasonable aerodynamic loads and damping when compared to those of full-scale wind turbines, as well as wakes with a realistic geometry, velocity deficit and turbulence intensity. Moreover, models have been conceived to enable individual blade pitch, torque and yaw control, while a sufficient onboard sensor equipment of the machine, providing measurements of rotor azimuth, main shaft loads, rotor speed and tower base loads, enables the testing of both wind turbine and wind farm control strategies.

Each *G1* model is equipped with three blades whose pitch angles can be varied by means of brushed motors housed in the hollow roots of the blades and commanded by dedicated electronic control boards housed in the hub spinner. Electrical signals from and to the pitch control boards are transmitted by a through-bore 12-channels slip ring located within the rectangular carrying box holding the main shaft. A torque sensor allows for the measurement of the torque provided by a brushless motor located in the rear part of the nacelle, which is operated as a generator by using a servo-controller. An optical encoder, located between the slip ring and the rear shaft bearing, allows for the measurement of the rotor azimuth. The tower is softened at its base by machining four small bridges, on which strain gauges are glued so as to measure fore-aft and side-side bending moments. Aerodynamic covers of the nacelle and hub ensure a satisfactory quality of the flow in the central rotor area.

Each *G1* model is controlled by an *M1 Bachmann* hardware real-time module. Similarly to what is done on real wind turbines, collective or individual pitch-torque control laws are implemented on and real-time executed by the control hardware. Sensor readings are used online to properly compute the desired pitch and torque demands, which are in turn sent to the actuator control boards via analog or digital communication.

2.3. The short-range WindScanner Lidars

The two short-range WindScanners R2D2 and R2D3, installed near the section walls upwind of the turbine models (see figure 3), are continuous-wave, coherent Doppler Lidars that can provide averaged wind speeds at rates up to 390 Hz. The measurement range is defined by the focus location which is motor controlled between about 9 m and 150 m. The longitudinal line-of-sight sampling volumes can become very small at short ranges, e.g. about 10 cm probe length at a 10 m focus distance, thus the WindScanners were placed as close as possible to the measurement area of interest. The laser beam can be freely steered within a cone with a full opening angle of 120° by the use of two prisms. The two prism motors and the focus motor in each system are synchronously steered by a common central motion controller that steers all the six motors such that the two focused laser beams are synchronously following a common scanning trajectory. The laser beam focus point of each WindScanner was pre-calibrated at DTU and the

location and orientation of the WindScanners relative to the wind tunnel and the wind turbines were achieved by inclination measurements and a Leica total station in combination with well localised rotating hard targets that give a distinct Doppler Lidar return signature. Additional verification of the measurement locations was done by the use of infrared sensitive equipment.

Each Lidar measures a projected line-of-sight component of the three-dimensional wind velocity vector. From two temporally and spatially synchronised line-of-sight measurements v_{LOS}, the u- and v-components of the wind speed, defined along and lateral to the main wind direction respectively, can be calculated by solving the linear equation system in Eq. (1):

$$\begin{bmatrix} \cos(\chi_1)\cos(\delta_1) & \sin(\chi_1)\cos(\delta_1) \\ \cos(\chi_2)\cos(\delta_2) & \sin(\chi_2)\cos(\delta_2) \end{bmatrix} \begin{bmatrix} u \\ v \end{bmatrix} = \begin{bmatrix} v_{LOS_1} \\ v_{LOS_2} \end{bmatrix} \tag{1}$$

In this linear system, the influence of the vertical wind component w is neglected. A third Lidar would be needed to evaluate this additional component. The horizontal and vertical scanning angles of a Lidar system are the azimuth χ and elevation δ angles, respectively. Because the Lidar scan heads are located slightly higher than the turbine hub height, small negative elevation angles $\delta < 3°$ had to be used. It is assumed that this causes an insignificant contamination of the result by the w-component.

2.4. The hot wire probe

A tri-axial Dantec 55R91 (see figure 4) hot wire probe was mounted on an automatic traversing system and provided 2500 Hz measurements of the three-dimensional wind speed vector in the wind tunnel. The three wires of the hot wire probe form an orthogonal system with respect to each other and are also positioned orthogonally to the prongs of the probe for increased accuracy. The effective sensor length of each of the wires is 1.25 mm. The hot wire anemometer had been calibrated in a dedicated open circuit wind tunnel at PoliMi before.
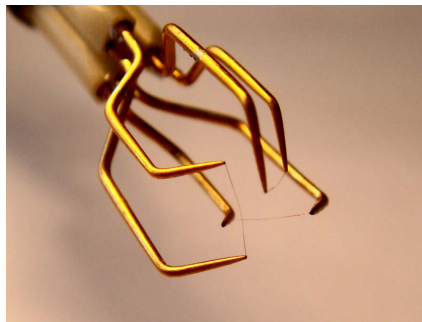

Figure 4. The tri-axial Dantec 55R91 hot wire probe.

2.5. Measurement examples

The measurement campaign covered several scenarios. In this paper, only relevant examples from the three main types of measurements are presented to illustrate the capabilities:

(i) *Comparison between Lidar and hot wire probe measurements*: The Lidar beams were focused as closely to the hot wire as practically possible, i.e. without influencing the hot wire probe due to heating by the laser beams on the one hand, or blocking the view of the Lidars with the hot wire probe and the traversing system on the other. The focus offset was chosen to be 2 cm. A series of different points in the wind tunnel were measured by both anemometers for a duration of 2 minutes each. In this case, the data of a single point at $x = 2.23$ m, $y = 0.88$ m, $z = 0.83$ m is considered for analysis. The wind turbines were

idling at approximately 80 rpm and this is assumed to have a negligible effect on the flow at the considered measurement point.

(ii) *Measurement of wake profiles along a line*: The Lidars performed measurements back and forth along crosswind lines at several distances downstream of the first wind turbine at hub height and spanning $\pm 3.5D$ around the wake centre. The complete line was covered every 1 s with equally sampled measurements. In the case presented, a wake profile at a $3D$ downstream distance of the first wind turbine is analysed. All turbines are operating under rated conditions. The first and second turbines have yaw offsets of $20°$ and $10°$, respectively.

(iii) *Measurement of horizontal wake area scans*: The full area containing the three wakes of the model turbines were mapped by the Lidars by iterating through the scanning pattern already indicated in figure 3. The scans cover an area of 7 by 13 m every 18.5 s. Multiple scans were averaged to resolve the mean wake features. All turbines are operating under rated conditions and have no yaw offset.

The inflow conditions were regulated to be constant. The free-stream wind speed and the turbulence intensity, both at hub height, were $u_0 = 5.67$ m s^{-1} and $TI = 5\%$, respectively. The vertical wind profile corresponded to a power law profile with shear exponent $\alpha = 0.08$.

3. Results

3.1. Comparison between Lidar and hot wire probe measurements

The first step of the Lidar campaign in the wind tunnel was to establish a quantitative measure of the accuracy of the Lidars with respect to the commonly applied devices in such an environment, i.e. hot wire anemometers. Here, the established hot wire probe served as a validation for the Lidar measurements. In order to compare the devices directly with each other, the hot wire probe data recorded at 2500 Hz has been averaged to match the Lidar measurement frequency of 390 Hz. Subsequently, the data of both devices was averaged to 1 Hz and compared again.

In table 1 the mean (μ) and standard deviation (σ) of the u-, v-, and w-components from a single 2-minute point measurement time series of both systems can be seen. The u-, v- and w-components of the hot wire are directly measured and the u- and v-components of the Lidars are derived from the line-of-sight measurements by applying Eq. (1). The w-component cannot be evaluated from the Lidar measurements in this case and is therefore neglected. The u-, v- and w-components are expressed in the x-, y- and z-direction of the Lidar reference frame, respectively, which is indicated in the wind tunnel configuration sketch (see figure 3). The hot wire probe measurements originally obtained in a different coordinate system were transformed into the Lidar frame of reference.

Table 1. Statistics of the wind speed components measured at a single point over a 2-minute time frame with the hot wire probe and the Lidars.

	Hot wire			Lidar	
	u	v	w	u	v
μ	5.67	-0.04	0.08	5.65	-0.03
σ	0.31	0.28	0.26	0.28	0.27

Correlation plots of both the u- and v-components are shown in figures 5 and 6, respectively. Although the regression line does not perfectly resemble $x = y$ and some scattering is visible, the measurements yielded very reasonable - especially for the considered sampling rate - goodness of fit coefficients of $R^2 = 0.777$ for the u-component and $R^2 = 0.633$ for the v-component. Possible reasons for the remaining scatter in the plot are:

- The probe volumes of the anemometers differ and they are not measuring in the exact same point or volume, so that different fluctuations are seen by the different devices.
- The contribution of the w-component on the measured v_{LOS} is neglected.
- There might be a small bias in the transformation between the different coordinate systems of the Lidars and the hot wire probe, causing a cross-contamination in the calculation of both wind speed components u and v.
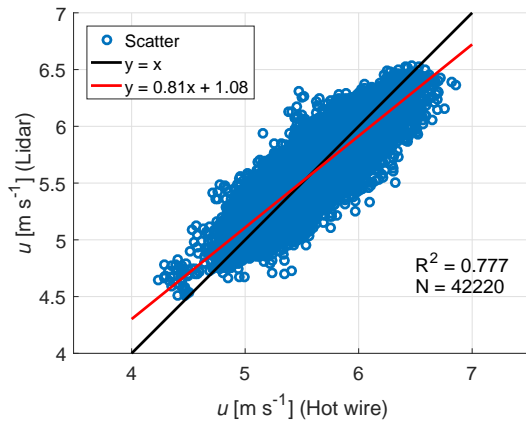

Figure 5. Correlation of the 390 Hz u-component.
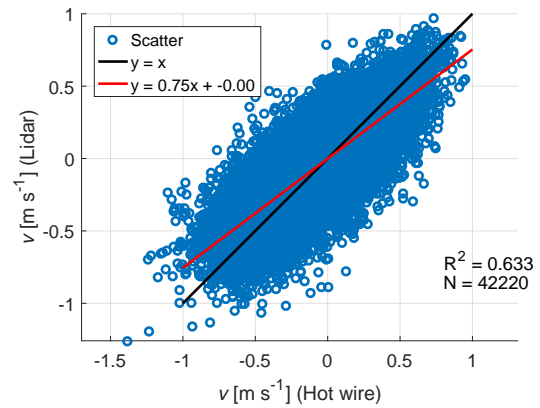
Figure 6. Correlation of the 390 Hz v-component.

The time series were subsequently further averaged to 1 Hz data. Showing both data sets in the same plot, figures 7 and 8 display the u- and v-components, respectively. On this time scale, it can be concluded visually that the measurements correlate very well.
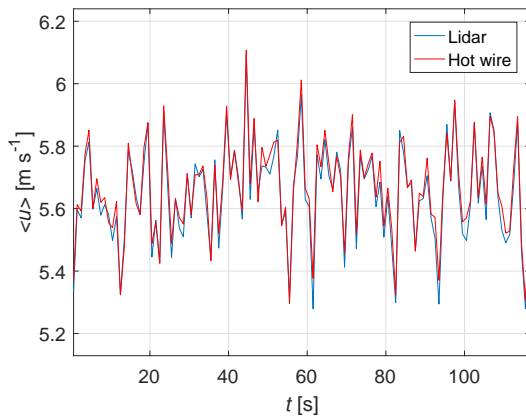

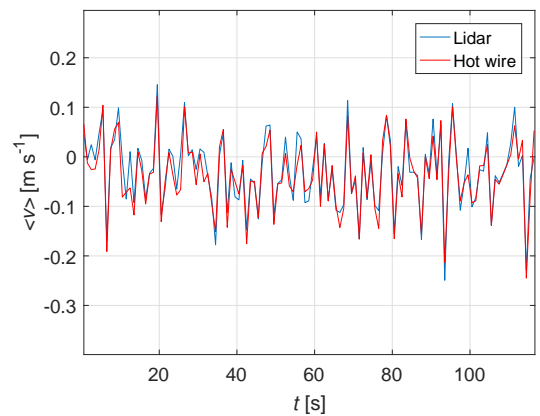**Figure 7.** Visual comparison of the 1 Hz averaged u-component.

Figure 8. Visual comparison of the 1 Hz averaged v-component.

The 1 Hz averaged u- and v-components in figures 7 and 8 were correlated with each other, as shown by figures 9 and 10.
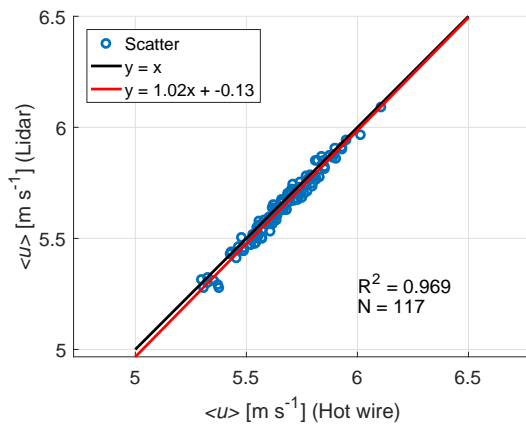
Figure 9. Correlation of the 1 Hz averaged u-component.
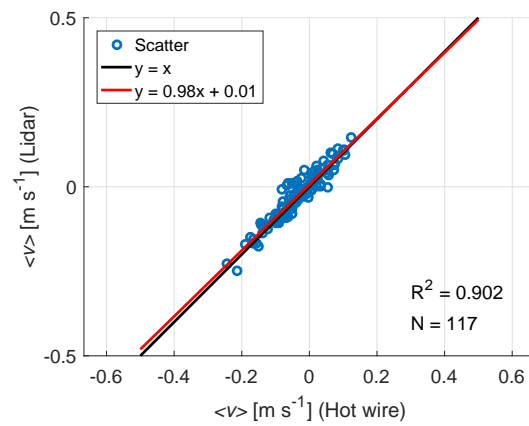
Figure 10. Correlation of the 1 Hz averaged v-component.

The mentioned effects that caused the scatter in the correlated 390 Hz data of figures 5 and 6 do not play a large role anymore after the data has been averaged to 1 Hz time series, since most of the very small scale fluctuations are omitted here. Correlating the 1 Hz averaged data now provided the goodness of fit coefficients of $R^2 = 0.969$ for the u-component and $R^2 = 0.902$ for the v-component, which can be regarded as a definite validation of the Lidar measurements in the wind tunnel. The fact that both components are estimated that well, is a confirmation of the good synchronisation of the WindScanners.
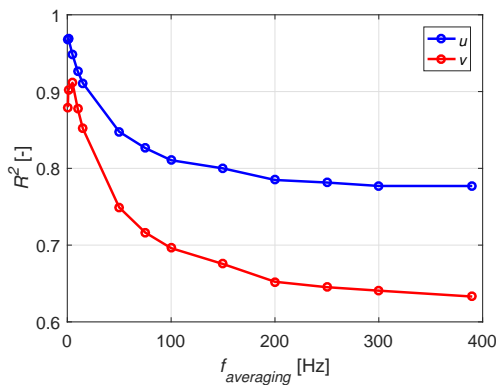

Figure 11. Goodness of fit parameter R^2 of the fit between the averaged u- and v-components of the Lidar and the hot wire as a function of averaging frequency.
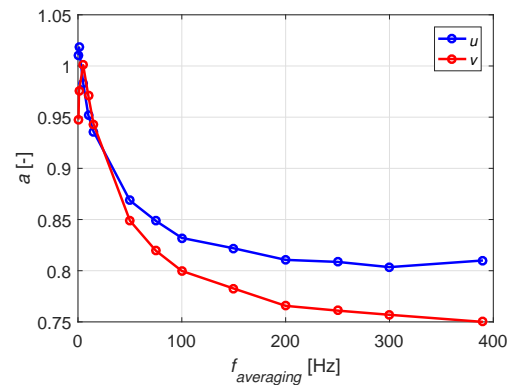
Figure 12. Slope a of the fit between the averaged u- and v-components of the Lidar and the hot wire as a function of averaging frequency.

Figures 11 and 12 show the influence of the averaging frequency on the goodness of fit R^2 and the regression line slope a, respectively. As expected, a better fit is yielded for lower averaging frequencies. In case of wake measurements, it is important that the Lidars are able to resolve the fluctuation scales induced by the wind turbines. Since the rated rotor speed is equal to 850 rpm, which is approximately 14 Hz, also the time series with this averaging rate were compared. The goodness of fit coefficients were $R^2 = 0.916$ for the u-component and $R^2 = 0.860$ for the v-component in this case.

To analyse the capability of measuring turbulence with Lidars [7], the spectrum of the u-component of both the Lidar and the hot wire are plotted in figure 13. Since the sampling frequencies of the hot wire probe and the Lidars are 2500 Hz and 390 Hz, respectively, the boundary of the plot was chosen to be the Nyquist frequency based on the Lidar, which equals 195 Hz. The Lidar measurements are based on the backscatter of aerosols in a small measurement volume with a length of approximately 10 cm in this case and therefore turbulent structures with a size smaller than this measurement probe volume are partly filtered out. By applying Taylor's Theorem [8] one can calculate that the Lidars can resolve temporal turbulence scales up to $\frac{1}{2}$·5.6 m s^{-1}/0.1 m = 28 Hz in this case. This line is marked in figure 13. It can be seen that the Lidar indeed shows less power in the spectrum than the hot wire for the upper frequency range. The drop in the slope of the spectrum does not exactly coincide with the 28 Hz frequency mark, because the intrinsic Lorentzian spatial weighing function of a continuous-wave Lidar extends beyond the defined bounds of the probe length, therefore also acting as a filter on lower frequencies. The effect of spatial weighing is explained in detail in [9]. Also combining measurements from two Lidars that each have a different probe volume, causes an even larger effect of averaging out small turbulence scales over a more complex volume.
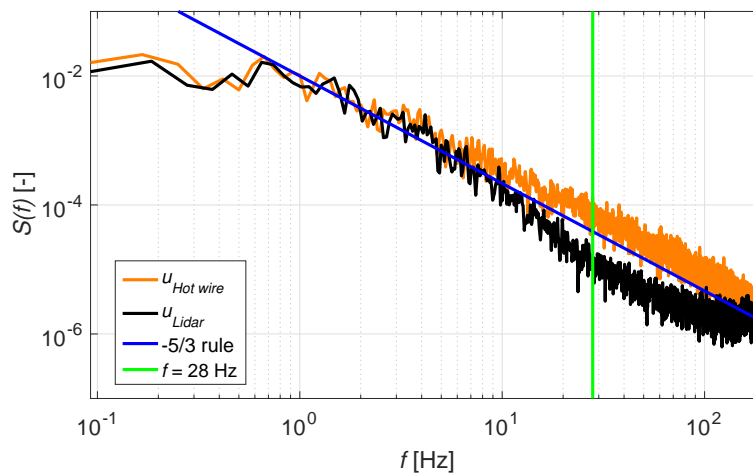

Figure 13. Turbulence spectrum of the u-component.

3.2. Measurement of wake profiles along a line

In figures 14 and 15, the respective u- and v-components of the wind speed evaluated from the line-of-sight measurements of both Lidars of the transverse wake profile at hub height at a distance of $3D$ downstream of the first turbine can be seen. Both components are normalised with respect to the free-stream velocity $u_0 = 5.67$. The data availability was 87.9%, due to the blockage effect of the wind turbine blades. All single measurements recorded with 390 Hz over a 1-minute period are plotted, as well as a bin averaged line with its standard deviation ($\pm 1\sigma$) bounds. The scatter of the measurements is reasonable and a smooth wake profile is produced. It is interesting to note that the v-component is almost zero on average, but it has a highly turbulent behaviour at the wake boundaries. This could be caused by tip vortices as well as the high velocity gradient at the boundaries of the wake.
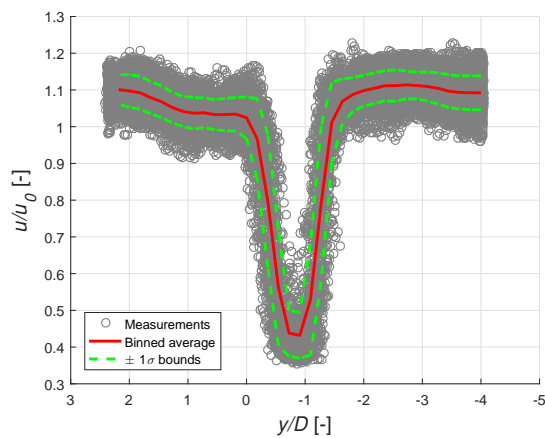
Figure 14. Wake profile expressed in the evaluated u-component, at $3D$ behind the first turbine with a $20°$ yaw angle.
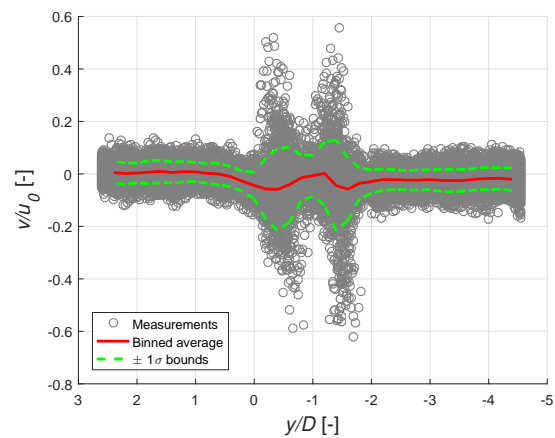
Figure 15. Wake profile expressed in the evaluated v-component, at $3D$ behind the first turbine with a $20°$ yaw angle.
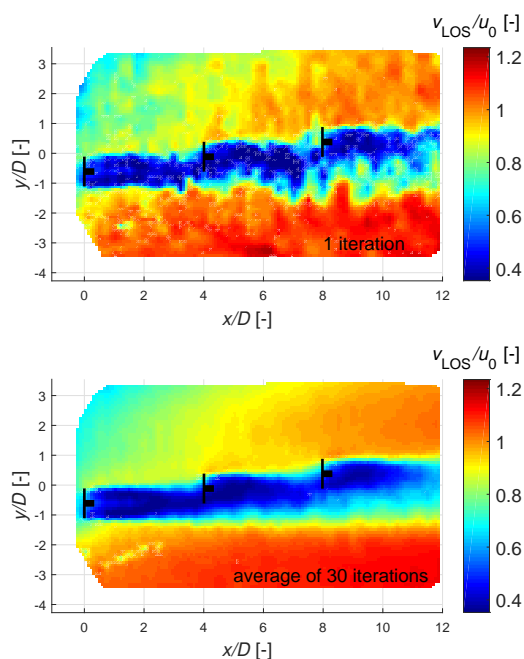

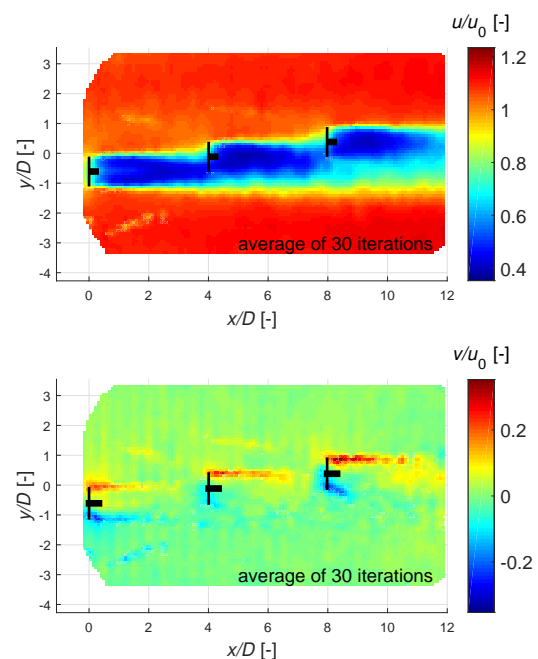**Figure 16.** Wake wind field expressed in the line-of-sight component of R2D3.

Figure 17. Wake wind field expressed in the evaluated u- and v-components.

3.3. Measurement of horizontal wake area scans
The flexibility of the WindScanners allows for programming synchronised scan patterns that cover any desired plane or volume in space. The scanning pattern sketched in figure 3 was used to map a horizontal plane at hub height containing the wake of all three wind turbines. Note that at the far end of the scan, the Lidar units are measuring at a focus distance of about 20 m, which results in a probe length of about 50 cm locally. In figure 16 the normalised line-of-sight

component measured by R2D3 is plotted, as the result of one scan iteration (upper) and as an average of 30 scan iterations (lower). This amount of iterations corresponds approximately to a 10-minute period. Although some blocking of the data is expected from the moving wind turbine blades, still the measurement availability after filtering of 89.4% is satisfying. The normalised u- and v-components, calculated through Eq. (1), are plotted in figure 17. It illustrates that the Lidars are successful in determining local 2D effects in wind turbine wake structures. The plot of the u-components shows a smooth and overlapping triple wake, enabled by the low turbulence in the wind tunnel. The non-zero local v-components are indicating the initial flow expansion in the induction zone of each of the turbines, as well as tip vortex effects on the wake boundary in the wakes. Interesting to note is that these effects are well visible in the upper part of the plot, whereas in the lower part of the wake these effects are averaged out due to the larger turbulence in the region where the wakes from the three turbines partly overlap.

4. Conclusions

A first measurement campaign with short-range synchronised Lidar WindScanner measurements in a wind tunnel demonstrated that this technology can be used to measure both the wind tunnel mean flow and turbulence as well as wake profiles of scaled wind turbines. Validation was performed successfully by comparing the Lidar measurements with commonly used hot wire probes. Because of the Lidar measurement principle, between 10-15% of the data is lost due to the moving wind turbine blades in the measurement region. Additionally, the Lidar systems cannot resolve the smallest turbulence scales due to the finite measurement probe volumes which are significantly larger than those of the hot wire probes. However, Lidar as a remote sensing application has the significant benefit that it does not influence the flow by its presence, contrary to the hot wire probes, which have to be mounted on a beam structure that potentially disturbs the flow. Also, the WindScanner technology enables scanning and mapping of entire two-dimensional horizontal and vertical wind fields within seconds to minutes. It is therefore our conclusion that scanning wind Lidars have significant potential for future wind tunnel measurement applications.

References
[1] Bottasso C L, Campagnolo F and Petrović V 2014 *Journal of Wind Engineering and Industrial Aerodynamics* **127** 11–28
[2] Rockel S, Camp E, Schmidt J, Peinke J, Cal R B and Hölling M 2014 *Energies* **7** 1954–1985
[3] About WindScanner Official Webpage Accessed: 1/6/2016 URL `http://www.windscanner.eu/About-WindScanner`
[4] Wagner R, Vignaroli A, Angelou N, Sathe A, Forsting A R M, M, Sjöholm and Mikkelsen T 2015 *DEWEK 2015, Bremen*
[5] Simley E, Angelou N, Mikkelsen T, Sjöholm M, Mann J and Pao L Y 2016 *Journal of Renewable and Sustainable Energy* **8**
[6] Zasso A, Giappino S, Muggiasca S and Rosa L 2005 Optimization of the Boundary Layer Characteristics Simulated at Politecnico di Milano Boundary Layer Wind Tunnel in a Wide Scale Ratio Ranges Tech. rep. Dipartimento di Meccanica - Politecnico di Milano
[7] Sathe A and Mann J 2013 *Atmos. Meas. Tech.* **6** 3147–3167
[8] Taylor G I 1938 *Proc. Roy. Soc. London* **164** 476–490
[9] Sjöholm M, Mikkelsen T, Mann J, Enevoldsen K and Courtney M 2009 *Meteorologische Zeitschrift* **18**